Benchmark Thermodynamic Contributors to the Growth and Decay of the Regional Extreme Surface Temperature

DONG WAN KIM,[a] SUKYOUNG LEE,[a] JOSEPH P. CLARK,[b] AND STEVEN B. FELDSTEIN[a]

[a] *Department of Meteorology and Atmospheric Science, The Pennsylvania State University, University Park, Pennsylvania*
[b] *Program in Atmospheric and Oceanic Sciences, Princeton University, Princeton, New Jersey*

(Manuscript received 16 June 2023, in final form 22 December 2023, accepted 31 January 2024)

ABSTRACT: A thermodynamic energy budget analysis is applied to the lowest model level of the ERA5 dataset to investigate the mechanisms that drive the growth and decay of extreme positive surface air temperature (SAT) events. Regional and seasonal variation of the mechanisms are investigated. For each grid point on Earth's surface, a separate composite analysis is performed for extreme SAT events, which are days when temperature anomaly exceeds the 95th percentile. Among the dynamical terms, horizontal temperature advection of the climatological temperature by the anomalous wind dominates SAT anomaly growth over the extratropics, while nonlinear horizontal temperature advection is a major factor over high-latitude regions and the adiabatic warming is important over major mountainous regions. During the decay period, advection of the climatological temperature by the anomalous wind sustains the warming while nonlinear advection becomes the dominant decay mechanism. Among diabatic heating processes, vertical mixing contributes to the SAT anomaly growth over most locations while longwave radiative cooling hinders SAT anomaly growth, especially over the ocean. However, over arid regions during summer, longwave heating largely contributes to SAT anomaly growth while the vertical mixing dampens the SAT anomaly growth. During the decay period, both longwave cooling and vertical mixing contribute to SAT anomaly decay with more pronounced effects over the ocean and land, respectively. These regional and seasonal characteristics of the processes that drive extreme SAT events can serve as a benchmark for understanding the future behavior of extreme weather.

KEYWORDS: Extreme events; Heat wave; Surface temperature

1. Introduction

Understanding the mechanisms that drive the observed surface air temperature (SAT; an elevation close to 2 m above the surface) anomalies is important because it helps us understand and predict anomalous weather events such as heat waves, which are a growing concern. The mechanisms proposed to date to explain temperature anomalies include anomalous surface heat flux (Yeo et al. 2019), which can be influenced by land–atmosphere coupling (Seneviratne et al. 2006), sinking motion and enhanced solar radiation under high pressure (Wulff et al. 2017), horizontal temperature advection (Clark and Feldstein 2020a, 2022), changes in downward infrared radiation (Gong et al. 2017), or some combination of these mechanisms (Lau and Kim 2012; Kim and Lee 2022). The same processes can also lead to the development of extreme anomalous temperatures (Bieli et al. 2015; Zschenderlein et al. 2019; Bartusek et al. 2022). While these studies provide useful insights, they focused on particular events or teleconnection patterns occurring over a limited geographical location. Thus, it remains an open question if those mechanisms can be applied to explain the cause of typical temperature anomalies at all other geographical regions across the globe and at other seasons.

There have been studies that examined the temperature probability distribution at all grid points over the globe in the context of skewness and the tail section of the distribution, and the physical processes that drive those characteristics of the distribution. Tamarin-Brodsky et al. (2019, 2020) found that horizontal temperature advection plays an important role in shaping the temperature skewness pattern under a global warming scenario. Other studies also found that temperature advection explains the temperature probability distribution across a large fraction of the midlatitudes (Linz et al. 2020), especially over the ocean (Zhang et al. 2022). Although not applied to the entire globe, horizontal temperature advection was also found to be important in the synoptic evolution of temperature extremes and skewness in the vicinity of the storm-track region (Garfinkel and Harnik 2017) and the development of regional cold extremes (Loikith and Neelin 2019). While these studies have provided useful insights into the understanding of the regional characteristics of the temperature probability distribution and extreme events, they have only considered the role of the horizontal temperature advection. Most of these studies also conducted their analyses in the lower troposphere, such as the 850- and 837-hPa levels. Although analysis at these levels may be suitable for exploring the large-scale atmospheric circulation associated with anomalous temperature, it is limited for revealing mechanisms that govern SAT anomalies, which are often influenced

Denotes content that is immediately available upon publication as open access.

Supplemental information related to this paper is available at the Journals Online website: https://doi.org/10.1175/JCLI-D-23-0368.s1.

Corresponding author: Dong Wan Kim, dxk582@psu.edu

DOI: 10.1175/JCLI-D-23-0368.1

by surface–atmosphere coupling. Moreover, the 850-hPa level may intersect with the surface of mountainous regions such as Greenland, the Tibetan Plateau, and the Rocky Mountains.

Knowledge of the mechanisms that contribute to temperature anomaly decay is critical for understanding the persistence of the temperature anomalies. However, most studies focus on the mechanisms that drive temperature anomaly growth, while temperature anomaly decay, which is not necessarily driven by the same processes that govern the growth of those anomalies (e.g., Clark and Feldstein 2020a, 2022), has often been overlooked.

In this study, we examine the mechanisms that drive the growth and decay of regional extreme SAT anomalies for both boreal summer [June–August (JJA)] and austral summer [December–February (DJF)] by applying a thermodynamic budget analysis at the lowest model level of ERA5 (Hersbach et al. 2020) for all individual grid points over the globe. ERA5 uses eta coordinates, which follow the surface elevation. As will be discussed in our analysis, the lowest model level of this coordinate system is used as the surface level. The lowest model level has an elevation that is close to 10 m above the surface (Berrisford et al. 2009; Setchell 2020). However, it has been shown that the temperature anomalies at this level are very similar to the anomalies in 2-m temperature, which is often regarded as SAT (Clark and Feldstein 2020a, 2022). Therefore, in this study, the temperature on the lowest model level will be regarded as the SAT.

A similar approach but from a Lagrangian point of view has recently been applied by Röthlisberger and Papritz (2023). However, in their analyses, horizontal temperature advection was not decomposed into linear and nonlinear components, which do not necessarily exhibit similar behaviors (Tamarin-Brodsky et al. 2019; Clark and Feldstein 2020a, 2022; Zhang et al. 2022), and the effects caused by radiative heating and by surface fluxes were not differentiated. Furthermore, the decay mechanism of the extreme temperature was not documented as well. In this research, we consider different components of the abovementioned processes as well as their behaviors during the decay period, which will provide a more comprehensive understanding of the regional characteristics of the extreme SAT anomaly development mechanisms.

The goal of this study is to provide information on which thermodynamic processes are responsible for positive SAT anomaly growth and decay during extreme temperature events at each grid point. The result identifies the benchmark thermodynamic contributors to the growth and decay of extreme SAT anomalies in each region. This benchmark mechanism allows one to determine whether a particular extreme weather event resembles a typical SAT anomaly event manifested in an extreme form and, more importantly, how such mechanisms may change under the current anthropogenic warming. Our main interest is the mechanism responsible for warm temperature extremes of the summer seasons of both hemispheres, but the results for the warm extremes of the winter seasons will also provide insights on how the proposed mechanisms may depend on the season.

In section 2, we provide detailed information about the data, the thermodynamic energy budget equation, and other methods used in this study of extreme SAT anomalies. In section 3, we introduce the regional characteristics of extreme JJA and DJF positive SAT anomaly growth and decay. The conclusions are presented in section 4.

2. Data and method

a. *Data, thermodynamic budget, and surface energy balance budget*

We used data from ERA5 to compute each term of the thermodynamic energy budget equation. As discussed above, the lowest model level in the ERA5 is used. All data have a horizontal resolution of 1.25° × 1.25° covering the time period of 1979–2021.

Following Clark and Feldstein (2020a), the anomalous thermodynamic energy budget equation is written as

$$\begin{aligned}\frac{\partial T'}{\partial t} = {} & (-\mathbf{u}'\cdot\nabla\overline{T} + \overline{\mathbf{u}'\cdot\nabla\overline{T}}) + (-\overline{\mathbf{u}}\cdot\nabla T' + \overline{\overline{\mathbf{u}}\cdot\nabla T'}) \\ & + (-\mathbf{u}'\cdot\nabla T' + \overline{\mathbf{u}'\cdot\nabla T'}) + (-\overline{\mathbf{u}}\cdot\nabla\overline{T} + \overline{\overline{\mathbf{u}}\cdot\nabla\overline{T}}) \\ & - \left(\dot{\eta}\frac{\partial T}{\partial\eta}\right)' + \left(\frac{\kappa T\omega}{p}\right)' + Q'_{\mathrm{SW}} + Q'_{\mathrm{LW}} \\ & + Q'_{\mathrm{Lat+Mix}} + \mathrm{Res}', \end{aligned} \tag{1}$$

where bars denote the seasonal cycle and primes denote an anomaly (deviation from the seasonal cycle). The seasonal cycle is defined as the calendar day mean climatology smoothed by retaining the first 10 harmonics. We obtained horizontal wind vectors ($\mathbf{u}$), temperature (T), vertical pressure velocity (ω), pressure (p), and temperature tendencies due to diabatic processes at the lowest model level to compute the terms in (1). The first six terms of the right-hand side of (1) indicate temperature tendency due to dynamical processes. Specifically, the first three terms are the advection of the climatological temperature by the anomalous wind, the advection of anomalous temperature by the climatological wind, and the advection of the anomalous temperature by the anomalous wind, respectively. The two terms $\mathbf{u}'\cdot\nabla\overline{T}$ and $\overline{\overline{\mathbf{u}}\cdot\nabla T'}$ are not equal to zero because the overbar indicates the smoothed seasonal cycle instead of the commonly used seasonal mean, although these terms are still very small (Clark and Feldstein 2020a). The fourth term also represents the effect of this smoothing process, and because this term is very small, it is not included in the main analysis. The fifth term, $-[\dot{\eta}(\partial T/\partial\eta)]'$, is the vertical advection in eta coordinates, and its numerical computation is explained in Clark and Feldstein (2020a). The sixth term, $(\kappa T\omega/p)'$, is the temperature tendency driven by adiabatic vertical motion. These dynamical terms were computed at 0000, 0600, 1200, and 1800 UTC separately, and were averaged to obtain the daily mean.

The seventh to ninth terms, Q'_{SW}, Q'_{LW}, and $Q'_{\mathrm{Lat+Mix}}$, are the temperature tendencies due to diabatic processes corresponding to shortwave radiation, longwave radiation, and the sum of latent heating and vertical mixing, respectively. ERA5 only provides total diabatic heating and the shortwave and longwave radiative diabatic heating. Therefore, the sum of latent heating and vertical mixing was computed as the difference

between the total diabatic heating and the radiative diabatic heating. While it is difficult to disentangle the relative contribution from latent heating and vertical mixing onto this term and that evaporative cooling near the surface level may not necessarily be negligible, given that the analysis is done at approximately 10 m above the surface, we assume that this term is dominated by vertical mixing. Therefore, for brevity, we will everywhere write "vertical mixing" even though it should be noted that the latent heating is included. We averaged 24-hourly diabatic heating data (0000–2400 UTC) to get the daily mean values. The last term is the residual term that is responsible for any difference between the combination of abovementioned terms and the total temperature tendency on the left-hand side of (1). There are a few potential reasons for the budget equation not being perfectly balanced. For example, horizontal diffusion is not included in the reanalysis model output, while the reanalysis model does include this term in its calculation. Also, there are reanalysis increments caused by the data assimilation processes (Clark and Feldstein 2020a; Clark et al. 2021). Nevertheless, this thermodynamic budget approach provides useful insights into the relative importance of different processes indicated in (1), which is the main goal of this study.

Apart from investigating the growth and decay of extreme SAT anomalies, we also investigated the development of skin temperature anomalies because an analysis of skin temperature anomalies aids in our understanding of some of the processes affecting the extreme SAT anomalies. By applying surface energy balance, the following equation can be derived:

$$T_s' = \frac{F_{\mathrm{lw}}'^{\downarrow} + F_{\mathrm{sw}}' + F_{\mathrm{sh}}' + F_{\mathrm{lh}}' + R'}{4\varepsilon_s \sigma \overline{T_s}^3}, \tag{2}$$

which states that skin temperature anomalies (T_s') are balanced by anomalies in downward longwave flux ($F_{\mathrm{lw}}'^{\downarrow}$), net shortwave flux ($F_{\mathrm{sw}}'$), net surface sensible heat flux (F_{sh}'), net surface latent heat flux (F_{lh}'), and a residual term (R') (Lesins et al. 2012; Lee et al. 2017; Clark and Feldstein 2020a). The residual term includes the storage term and additional processes such as heat conduction, oceanic horizontal heat transport, vertical mixing in the oceanic boundary layer, and the latent heat release associated with sea ice melting, terms which can be large over the ocean. All fluxes in this study are defined as positive being downward. Note that in the denominator we approximate the emissivity (ε_s) as 1.0; σ denotes the Stefan–Boltzmann constant and $\overline{T_s}$ is taken to be the seasonal (JJA or DJF) mean skin temperature.

b. Composite of anomalous events

We identified extreme SAT events at each grid point as occurring when the SAT anomaly is a local maximum (in time) and positive with an amplitude greater than the 95th percentile. These events are also separated from each other by at least 7 days. In other words, local maxima of a smaller amplitude that occur within a 7-day period of a large local maxima are discarded. This procedure is performed separately for JJA and DJF. Based on this procedure, approximately 70–100 extreme events for each season were identified at each grid point over extratropical land regions (Fig. S1 in the online supplemental material). We have composited the thermodynamic energy budget terms using these events. While lag day 0 of these events is when the SAT anomaly is largest, we present temperature tendencies at lag day −1 (+1) to examine the anomalous SAT growth (decay), as these lag days correspond to days with the strongest temperature tendencies over most grid points. We composited each budget term at each grid point for these lag days and assigned that composite value to the corresponding grid point. Therefore, the resulting maps in Figs. 1 and 3 (Figs. 4 and 6) show the contribution of specified processes to the growth and the decay of extreme SAT events, respectively, occurring at that specific grid point during the JJA (DJF) season.

3. Results

a. JJA analysis

1) Growth of positive SAT anomalies

We present the benchmark thermodynamic contributors to extreme SAT anomaly growth during the JJA season in Fig. 1. The positive SAT anomalies are generally stronger over the extratropical land regions (Fig. 1a). The summation of all the terms on the right-hand side of the budget equation (Fig. 1c) shows a similar pattern as the actual temperature tendency pattern (Fig. 1b). The difference between the two maps is shown in Fig. 1d. The budget is not perfectly balanced due to the factors mentioned in section 2. However, the difference between the two patterns is rather small, especially over extratropical land areas where extreme events have the largest impact on society. This indicates that the thermodynamic budget analysis can be used to identify the processes that cause the extreme SAT anomalies to grow.

The temperature tendency driven by the combination of all the dynamic terms largely accounts for the warming over most of the mid- and high-latitude locations in both hemispheres (Fig. 1e). The advection of the climatological temperature by the anomalous wind makes the largest contribution to the SAT anomaly development in the extratropics with a pronounced effect near the storm tracks of both the Northern Hemisphere (NH) and the Southern Hemisphere (SH; Fig. 1g). In contrast, the advection of the anomalous temperature by the climatological wind contributes to the SAT anomaly development over selected regions such as Greenland and the SH storm-track region, with its overall contribution being negligible in other regions (Fig. 1h). The nonlinear advection of the anomalous temperature by the anomalous wind contributes to positive SAT anomaly development over high-latitude regions (Fig. 1i). The summation of these three contributions (Fig. 1j) shows that horizontal temperature advection accounts for most of the dynamic contribution of the SAT anomaly development (cf. Figs. 1e,j). This important role of horizontal temperature advection on extreme SAT growth is in line with previous research that examined temperature probability distribution

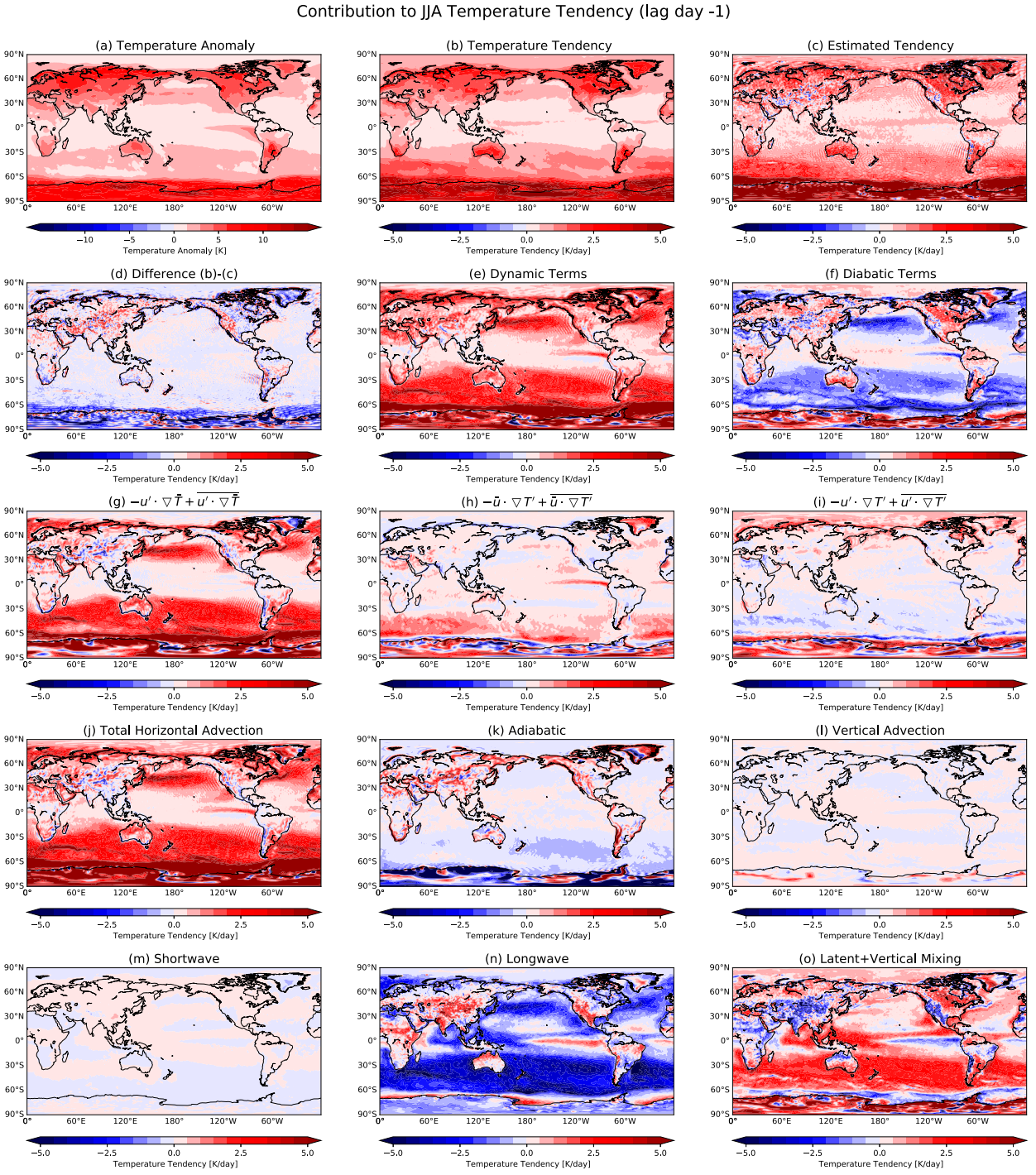

FIG. 1. Composite values of (a) temperature anomaly and (b)–(o) different temperature tendency terms during the lag day −1 of the JJA warm extreme events defined separately for each grid point (see text for details). Positive (negative) tendencies in (b)–(o) indicate that the corresponding processes drive (dampen) the growth of the temperature anomaly occurring at that grid point.

characteristics (Linz et al. 2020; Tamarin-Brodsky et al. 2019, 2020; Zhang et al. 2022).

While horizontal temperature advection plays a pronounced role over most locations, the tendency contributed by adiabatic vertical motion is in fact comparable to that of horizontal temperature advection over mountain ranges such as the Tibetan Plateau, the Rocky Mountains, the Andes, and Greenland (Fig. 1k). This term also contributes to the anomaly development over the Russian Far East, the west coast of North America, and in the vicinity of the Mediterranean Sea.

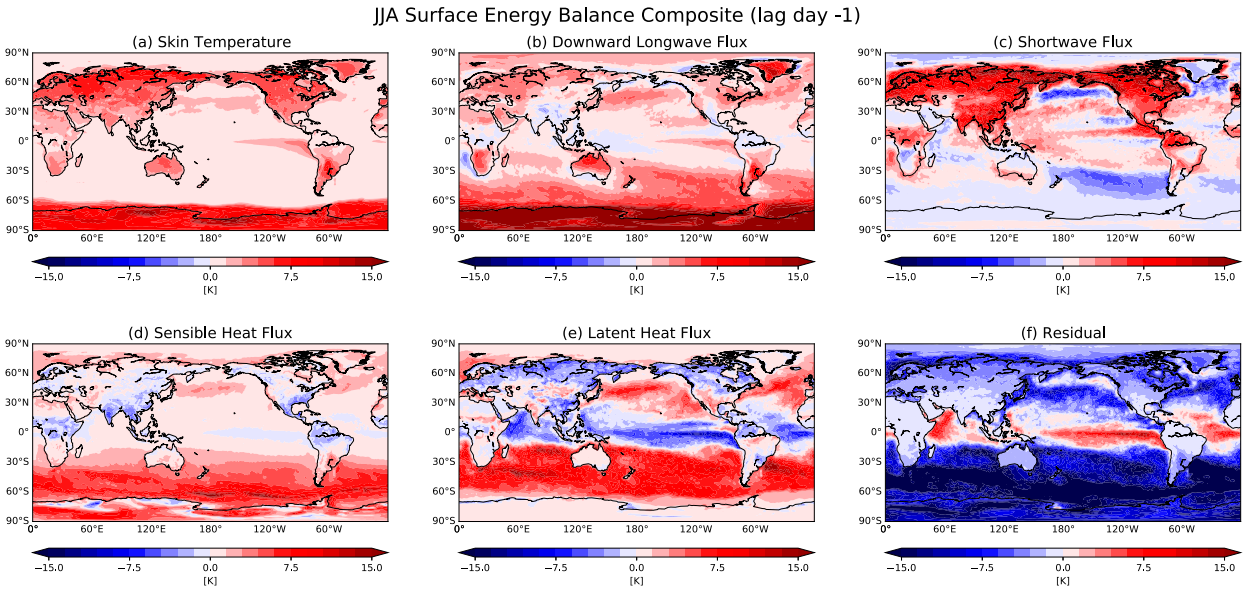

FIG. 2. Composite values of (a) skin temperature anomaly and (b)–(f) different surface flux terms during the lag day −1 of the JJA warm extreme events used for Fig. 1 (see text for details). Note that flux terms are normalized by $4\varepsilon_s\sigma\overline{T_s}^3$ to have a unit of kelvins.

The role of the adiabatic term over mountain ranges is consistent with the findings from Röthlisberger and Papritz (2023), who showed that strong adiabatic warming occurs over the slope side of the mountain, implying adiabatic vertical motion following the topography. The contribution by vertical advection is generally negligible (Fig. 1l). In summary, the dynamic contributions to extreme SAT anomaly growth can be characterized by a combination of three dominant processes. The advection of the climatological temperature by the anomalous wind dominates the SAT anomaly growth over the extratropics with additional support from the nonlinear advection over high-latitude regions and adiabatic warming over the mountain ranges.

Unlike the dynamic terms which contributed to extreme SAT anomaly growth over almost all regions except for a few locations in the tropics, the temperature tendency due to diabatic process shows a distinctive land–sea contrast as it warms most land areas while it hinders the anomaly growth over the extratropical oceans (Fig. 1f). Decomposing the total diabatic process into longwave radiation, shortwave radiation, and vertical mixing, we found that vertical mixing is the primary driver of the diabatic warming (Fig. 1o), while longwave radiation generally causes cooling (Fig. 1n). However, the roles that these two terms play reverses over some regions. Over climatologically dry regions such as northern Africa, the Tibetan Plateau, and western North America, longwave radiative heating contributes to the growth of the positive SAT anomalies while vertical mixing hinders the positive SAT anomaly growth. The effect of shortwave radiation is very small (Fig. 1m), as expected from the fact that the atmosphere is mostly transparent to shortwave radiation. These results indicate that diabatic processes also play an important role in the development of extreme SAT anomalies, with a role that can be as important as, or even greater, than that of dynamic processes over most NH land regions (cf. Figs. 1e,f). It is beyond the scope of this study to fully delve into the cause of these diabatic heating terms, but an analysis of the surface energy budget can provide useful insights (as discussed in section 2).

Composites of the skin temperature anomalies and surface fluxes are presented in Fig. 2. One day prior to an extreme SAT event (lag day −1), when the SAT tendency is strongest, the skin temperature anomalies are generally stronger over land than over ocean (Fig. 2a), and these anomalies are primarily balanced by the net downward shortwave flux especially in the NH (Fig. 2c) with the downward longwave flux playing a secondary role (Fig. 2b). The dominance of the shortwave flux in warming the surface is to be expected because most of the incoming shortwave radiation is absorbed by the surface. Over some areas, the spatial structure of the downward longwave flux (Fig. 2b) bears resemblance to that of the longwave diabatic heating at the lowest model level (Fig. 1n) but with an opposite sign. For example, there are strong anomalous downward fluxes over extratropical oceans in both hemispheres where longwave cooling at the lowest model level is also strong.

We present a schematic diagram (Fig. S2) to illustrate the connection between the downward longwave flux at the surface and the longwave flux divergence at the lowest model level. The arrows indicate longwave fluxes into and out of the layer surrounding the lowest model level, that is bounded by a 1/2 model level above and by the surface below. This schematic diagram indicates that after the atmosphere warms (right side of Fig. S2), both upward and downward longwave fluxes from the lowest model level layer increase (F_{out}, $F_{\text{atm}\to\text{ocn}}$). Concurrently, the flux into the lowest model level layer from

above also increases (F_{in}) while the upward flux from the ocean into the lowest model level layer ($F_{atm\rightarrow ocn}$) does not change much since the sea surface temperature remains relatively constant. As discussed in Clark and Feldstein (2022) (who analyzed SAT anomalies associated with the Pacific–North American teleconnection pattern), this is likely to cause an anomalous divergence of longwave heat flux at the lowest model level and consequently, pronounced longwave cooling at the lowest model level over the ocean (Fig. 1n).

The surface sensible heat flux anomalies are either close to zero or weakly negative over most of the NH land areas while over the SH storm-track regions the surface sensible heat flux anomalies are strongly positive (Fig. 2d). Over these land areas, this sensible heat flux pattern suggests that the anomalous skin temperature is larger than the anomalous SAT, likely due to the shortwave warming of the surface (Fig. 2c), while the picture is reversed over the austral winter Southern Ocean where advective warming of the air is strong (Fig. 1j) and shortwave radiation at the surface is weak. The surface latent heat flux anomalies are negative over most of the NH land areas, representing evaporative cooling of the surface with exceptions over the Tibetan Plateau and western North America (Fig. 2e). The opposite signs for these anomalies indicate that the latent heat flux dampens the skin temperature anomalies through evaporative cooling while such cooling is not efficient over climatologically dry regions. Over most NH land areas, these regions of negative (positive) anomalous latent heat fluxes coincide with regions of atmospheric warming (cooling) due to the vertical mixing (Fig. 1o).

The cooling by the residual term (Fig. 2f), which includes heat conduction and effects from sea ice and ocean circulation, balances the other terms' warming over most of the globe. Over land, the skin temperature is cooled through heat conduction. Whereas over the ocean, oceanic vertical and horizontal motion cools the ocean skin temperature over most regions. For example, regions of strongest cooling by the residual term over the Southern Ocean coincide with the region of a deep and narrow mixed layer (Li and Lee 2017; Li et al. 2018). It is also interesting that the residual term is positive in the eastern equatorial Pacific where the climatological oceanic horizontal heat flux is divergent (Forget and Ferreira 2019). Therefore, the positive residual term suggests that the anomalous warming in that region by the residual arises from a weakening of the oceanic horizontal heat flux divergence.

2) Decay of positive SAT anomalies

We next examine the characteristics of the thermodynamic energy budget terms during the decay period of lag day +1 (Fig. 3). While some processes simply mirror their growth pattern with opposite signs, there are notable differences as well. Over most of the land areas, both dynamic (Fig. 3e) and diabatic (Fig. 3f) terms drive the decay of the SAT anomalies. Over the extratropical oceans, however, the dynamic terms still sustain the anomalous warming. This sustained warming is largely due to the advection of the climatological temperature by the anomalous wind (Fig. 3g), which is similar in spatial structure but with a weaker magnitude compared to that of the growth period (cf. Figs. 1g and 3g). The advection of anomalous temperature by the climatological wind (Fig. 3h) shows an almost equal spatial structure but with opposite sign compared to that of the growth period (Fig. 1h), except over the eastern tropical Pacific, indicating that it contributes to the SAT anomaly decay over the SH storm-track region while its impact is rather limited over the NH.

Nonlinear temperature advection becomes one of the dominant drivers of the SAT anomaly decay as this process weakens the positive SAT anomalies over most of the extratropical land areas in both hemispheres (Fig. 3i). While adiabatic warming was important during the growth period, this process does not play an important role for the decay of the SAT anomalies (Fig. 3k). The longwave radiation maintains a similar spatial structure compared to that of the growth period as it helps (hinders) the anomaly decay over the ocean (dry land regions) (see Fig. 3n). This is likely due to the fact that the spatial structure of the positive SAT anomaly remains the same at lag day +1 (Fig. 3a). Vertical mixing generally mirrors its growth stage over the land but with an opposite sign contributing to the decay of the SAT anomaly (Fig. 3o). The overall results indicate that, among the dynamic processes, nonlinear temperature advection contributes to SAT anomaly decay over the land and ocean, whereas among the diabatic heating processes, longwave radiative cooling contributes to SAT anomaly decay over the oceans while vertical mixing contribute to SAT anomaly decay over the land. It is also interesting that the advection of the climatological temperature by the anomalous wind, unlike other terms, sustains the warming mechanism, indicating that this process plays an important role on the persistence of the extreme temperature events.

b. *DJF analysis*

1) Growth of positive SAT anomalies

In this subsection, the contribution of each term in the thermodynamic energy budget equation is explored for extreme SAT events that occur during DJF. Although most of the processes that characterize DJF SAT extremes are similar to those that characterize JJA SAT extremes, there are some noticeable differences.

Figure 4 shows a composite of the thermodynamic energy budget for DJF. Extreme SAT anomalies during DJF attain their largest amplitudes over the land and the Arctic of the NH (Fig. 4a). Although the estimated tendency (Fig. 4c) captures the actual temperature tendency (Fig. 4b), it generally overestimates the actual temperature tendency over NH land areas and the Arctic while the difference is very small in the SH and the oceans (Fig. 4d). We hypothesize that the error caused by the analysis increment being stronger in the winter hemisphere, though it is beyond the scope of this study to investigate this seasonal dependence of the overall balance of budget terms. Similar to the JJA season, the dynamic terms strongly contribute to positive SAT anomaly development over the extratropics (Fig. 4e) while the diabatic terms again show the distinctive land–sea contrast pattern (Fig. 4f).

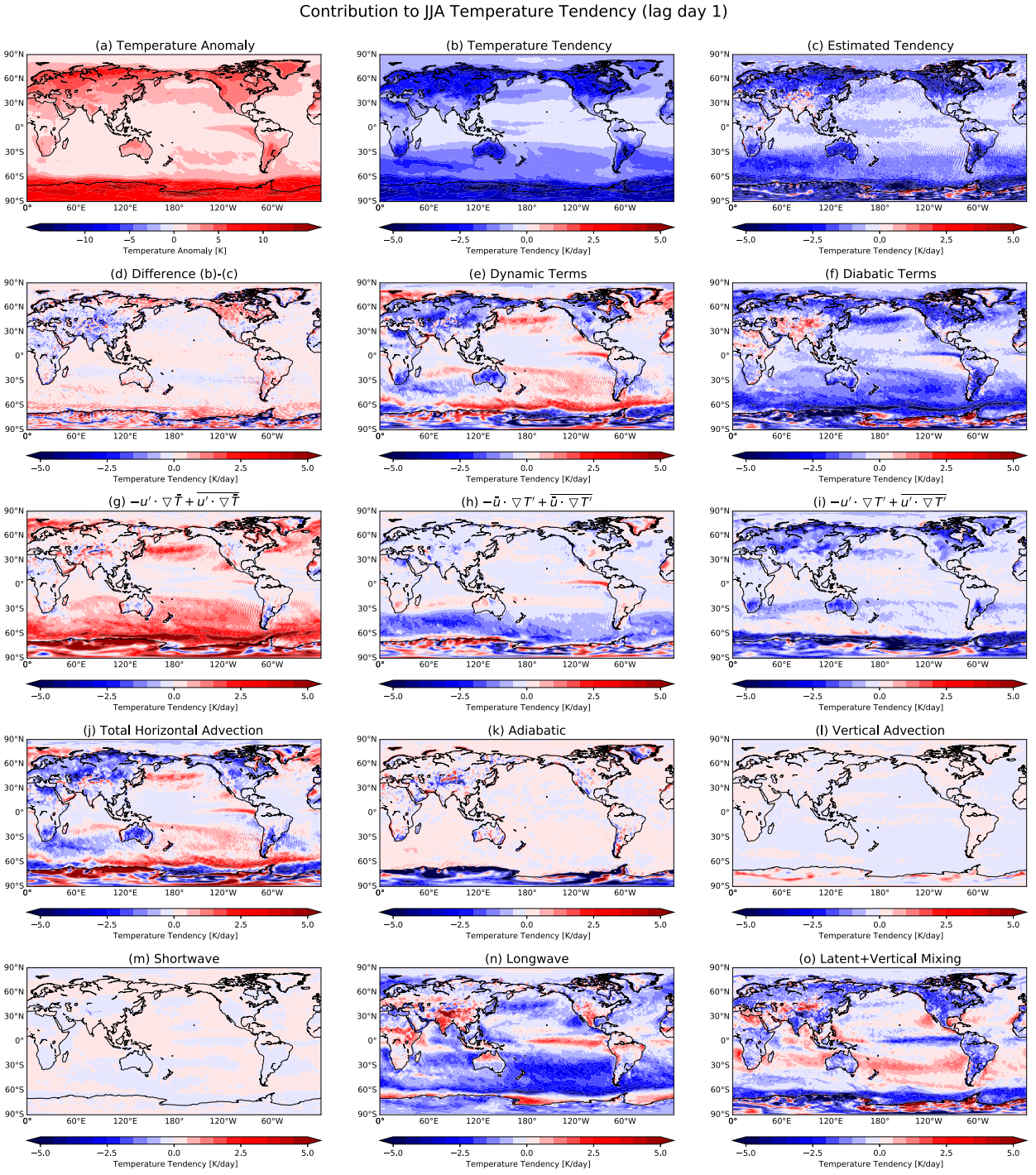

FIG. 3. As in Fig. 1, but during lag day +1 of the JJA events. Positive (negative) tendencies in (b)–(o) indicate the corresponding processes dampens (help) the decay of the temperature anomaly at that grid point.

The advection of the climatological temperature by the anomalous wind accounts for the SAT anomaly growth over the extratropics, most prominently over the storm-track regions of both hemispheres and near the Barents–Kara Seas (Fig. 4g). The advection of the anomalous temperature by the climatological wind plays an important role over the western boundaries of the Pacific and Atlantic Ocean basins and Greenland while it dampens the SAT anomaly growth over the Barents–Kara Seas (Fig. 4h). This process also contributes to the warming over the SH storm track but its amplitude is rather weak compared to that of the JJA season. The nonlinear temperature advection term accounts for warming over

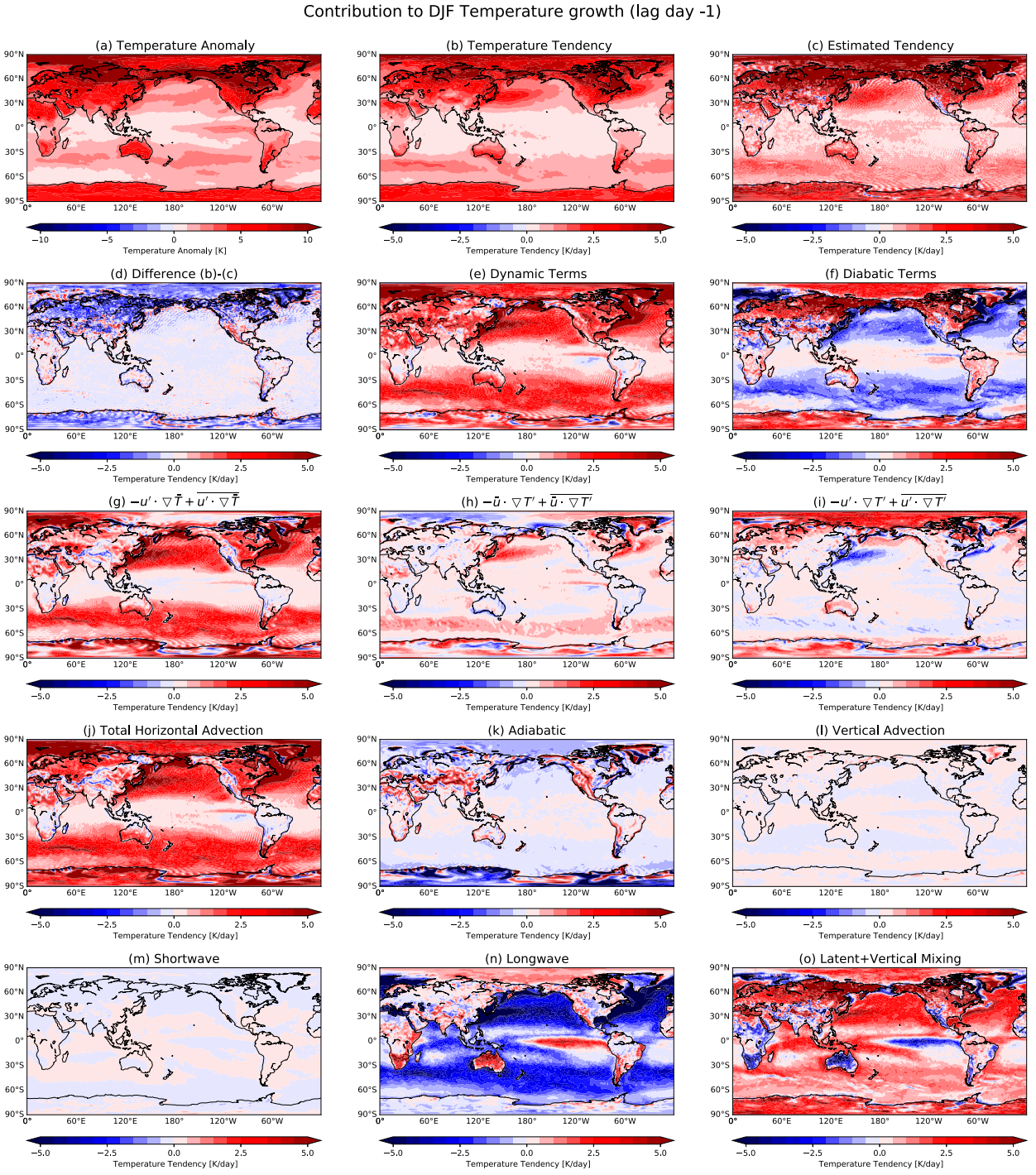

FIG. 4. As in Fig. 1, but during lag day −1 of the DJF events.

most of the Arctic during DJF while it dampens SAT anomaly growth over the western boundaries of the two major NH ocean basins (Fig. 4i). Accordingly, the combination of these three terms highlights the important role of horizontal temperature advection over most of the extratropical regions (Fig. 4j). Compared to JJA, the role of horizontal advection is intensified (weakened) over the NH (SH). This seasonal difference is likely explained by the stronger atmospheric circulation and temperature gradient of the winter hemisphere. During the DJF months, the adiabatic term acts to increase the SAT over mountain regions (Fig. 4k). However, unlike during JJA, the adiabatic term dampens the SAT anomalies over high-latitudes and the Arctic. This adiabatic cooling is possibly a response to the strong positive horizontal temperature advection occurring

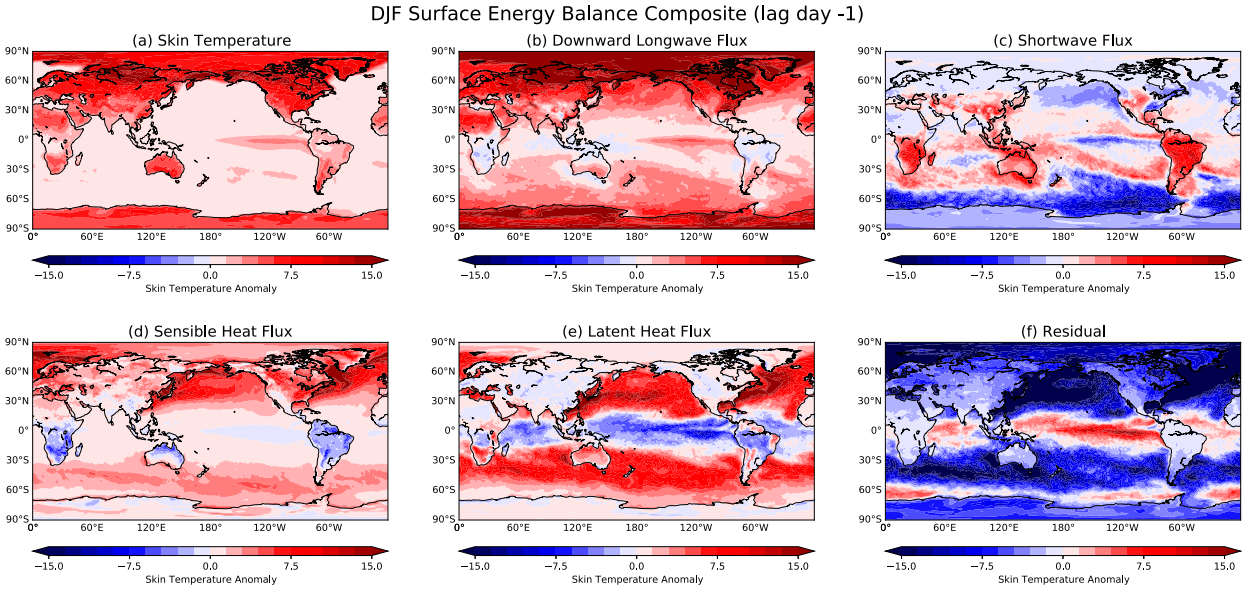

FIG. 5. As in Fig. 2, but during lag day −1 of the DJF events.

at high latitudes (Fig. 4j), as the vertical motion explained by quasigeostrophic theory is upward with warm-air advection, which would result in adiabatic cooling. As in JJA, the role of vertical advection is also negligible during DJF months (Fig. 4l).

The general characteristics of the DJF diabatic heating also resembles that of the JJA season. Among the three diabatic heating terms, longwave radiative heating generally hinders the anomaly growth, especially over the oceans (Fig. 4n), and vertical mixing largely contributes to anomaly growth over most of the globe (Fig. 4o). The shortwave radiative heating does not directly impact the SAT (Fig. 4m). While these behaviors are similar to those of JJA, there are some regional differences that contrast with the JJA findings. First, longwave radiative heating, while predominantly cooling oceanic air, warms the air over South Africa, Australia, western South America, the eastern tropical Pacific, and the Arctic. Vertical mixing, which largely accounts for the warming of most NH land areas (Fig. 4o), dampens the anomaly growth over SH land regions where longwave heating is prevalent. Notably, these SH land areas are climatologically arid regions. Therefore, similar to our previous finding that longwave warming (vertical mixing) contributes to (negates) summertime warming over NH arid regions (Figs. 1n,o), the two processes play a similar role in the positive SAT anomaly development of the arid regions during austral summer (Figs. 4n,o).

The skin temperature anomaly during DJF (Fig. 5a) is primarily governed by the downward longwave flux (Fig. 5b) while the shortwave flux contributes to skin temperature anomaly growth equatorward of 45°N/S, with more pronounced effects over the SH (austral summer; Fig. 5c). The sensible heat flux composite shows anomalously downward fluxes in the NH and SH oceans with anomalously upward heat fluxes over SH land (Fig. 5d). The anomalously downward sensible heat fluxes in the NH are more pronounced over the western boundaries of the major ocean basins and the Barents–Kara Seas where temperature advection strongly drives the positive SAT tendency (Fig. 4j). Also, the anomalous upward surface sensible heat flux over the SH land areas suggests that the surface is anomalously warmer than the air at the lowest model level, likely due to strong shortwave flux at the surface (Fig. 5c). The surface latent heat flux anomalies are positive over the SH dry land areas (Fig. 5e). This positive surface latent heat flux anomaly occurs in the regions of cooling by vertical mixing (Fig. 4o), similar to the picture described for the NH dry land areas during JJA. However, over NH land regions during DJF, the latent heat flux anomalies are almost negligible and, therefore, are less likely to influence the SAT.

2) DECAY OF POSITIVE SAT ANOMALIES

During the decay period, advection of the climatological temperature by the anomalous wind sustains the warming, most notably over the northernmost parts of the Pacific, the Atlantic, and the Southern Ocean (Fig. 6g). The advection of the anomalous temperature by the climatological wind mirrors its growth period but with opposite sign as it contributes to the anomaly decay over the storm-track regions of the Pacific, the Atlantic, and the Southern Ocean while it hinders the anomaly decay over the Barents–Kara Seas (Fig. 6h). The nonlinear advection, similar to its JJA behavior, is largely responsible for the SAT anomaly decay over most of the NH with a very pronounced effect over the Arctic (Fig. 6i). The role of adiabatic process is again focused on the mountain regions such as the Rockies and the Tibetan Plateau (Fig. 6k), while vertical advection does not play an important role (Fig. 6l). Such characteristics of the abovementioned terms result in the dynamical process contributing to the decay of the SAT anomalies over most of the globe with exceptions

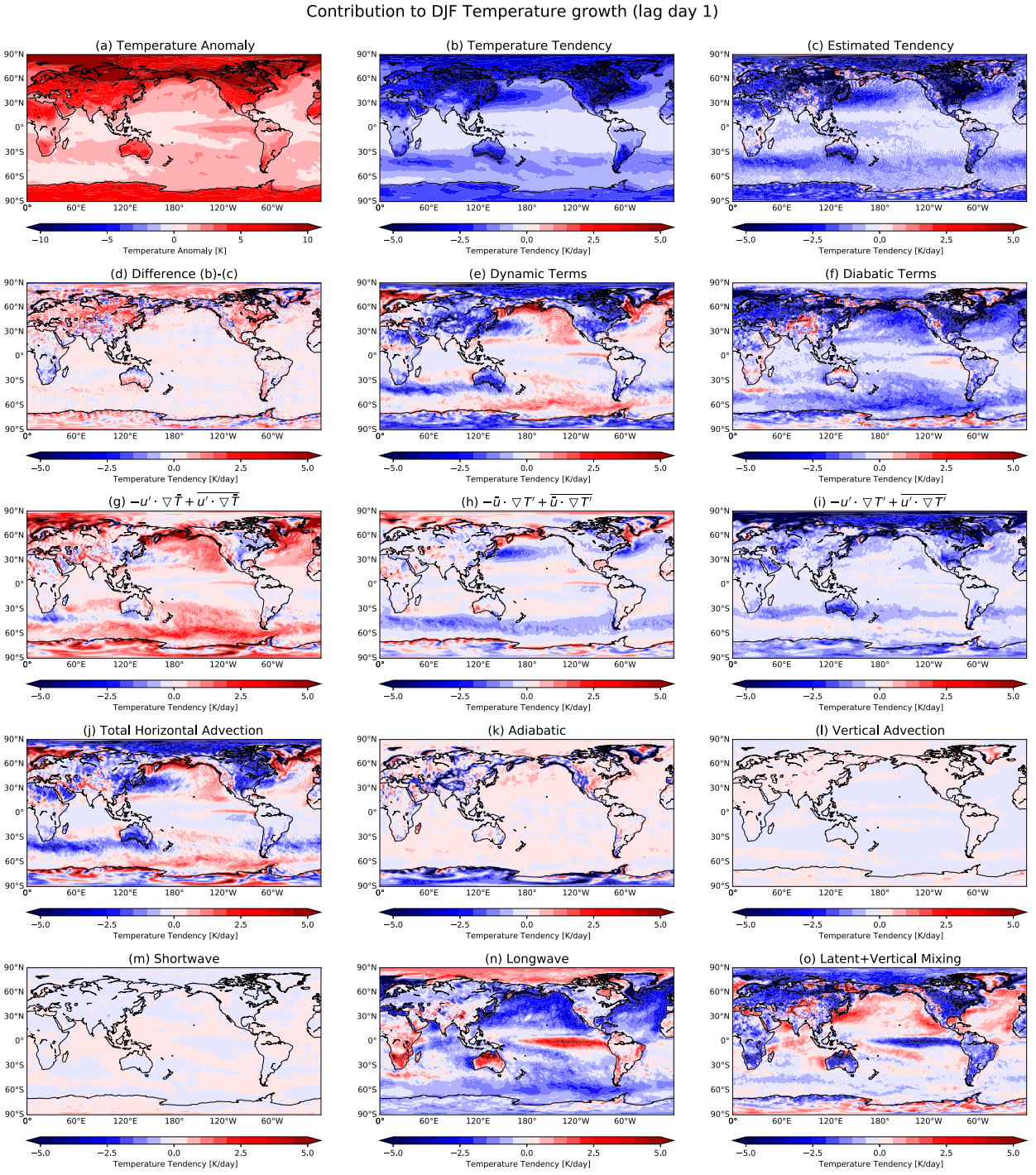

FIG. 6. As in Fig. 3, but during lag day +1 of the DJF events.

occurring over northern parts of the North Pacific, the North Atlantic, and the Southern Ocean (Fig. 6e). Among the diabatic heating terms, the longwave heating maintains its structure from the growth period, as it did during JJA, and largely accounts for the anomaly decay over the ocean (Fig. 6n). Vertical mixing is largely responsible for the anomaly decay over land (Fig. 6o). It is noteworthy to mention that the SAT anomaly development over the NH land by vertical mixing is similar to the Siberian warming and cooling mechanism during PNA events (Clark and Feldstein 2022). They found that the growth and decay of Siberian SAT anomalies occurred through vertical mixing which they argued as acting to relocate temperature anomalies from higher levels into the lowest model level.

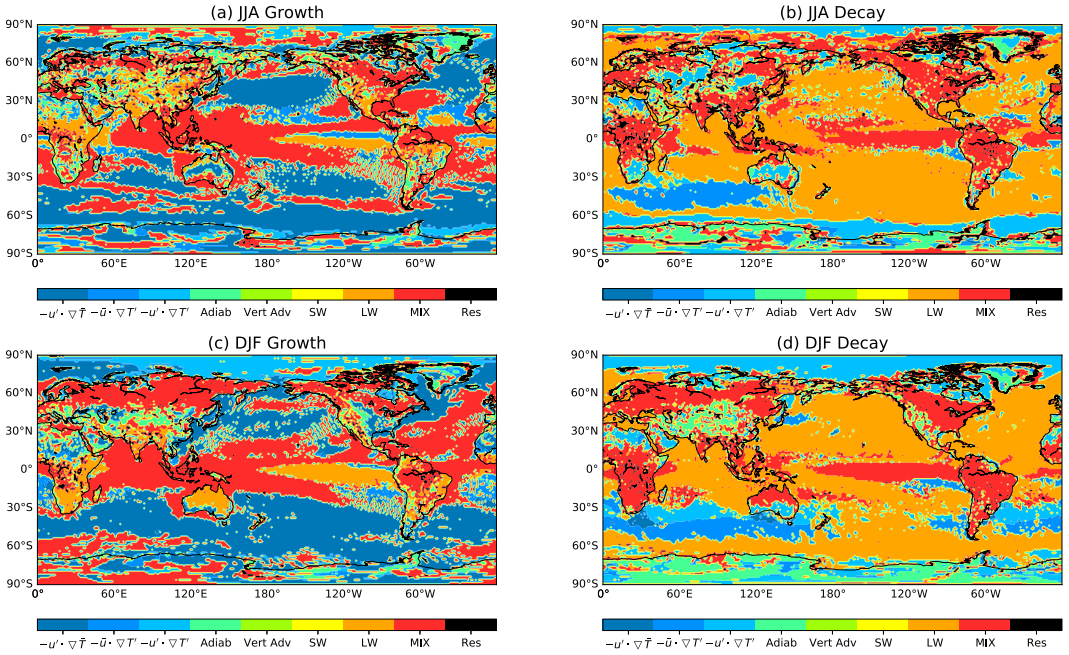

FIG. 7. The most important process for the growth and decay of the extreme SAT anomalies occurring at each grid point for the JJA and DJF seasons (see text for details). Blue, green, warm, and black colors indicate different components of horizontal temperature advection, adiabatic warming and vertical advection, diabatic heating terms, and the residual term, respectively.

4. Conclusions and discussion

In this study, we applied thermodynamic budget analyses to the SAT anomalies at each grid point to understand the processes contributing to extreme warming events over each region of the globe. Inspired by Fig. 3 of Röthlisberger and Papritz (2023), we summarize in Fig. 7 the most important process for the growth and decay of the extreme SAT events for each grid point by identifying the strongest positive (negative) tendency term during the growth (decay) period. These findings indicate that the role of the dynamical terms depends on the latitude and topography while the diabatic heating processes exhibit a distinctive land–sea contrast with specific characteristics as follows:

- The advection of the climatological temperature by the anomalous wind (dark blue) dominates the SAT anomaly development over the extratropical oceans except for the eastern North Atlantic during DJF, while nonlinear temperature advection (light blue) is the largest contributor to SAT growth in much of high latitudes, especially over the Arctic during DJF (Figs. 7a,c). However, during the decay period, these terms do not mirror their growth patterns, as the advection of the climatological temperature by the anomalous wind sustains the warming (this feature is not shown in Fig. 7) and nonlinear temperature advection becomes the largest contributor during the decay period over most of the Arctic Ocean (both seasons) and the subtropical southern Atlantic and Indian Oceans during DJF (Figs. 7b,d). Although it cannot be discerned in Fig. 7, there are still substantial secondary contributions from horizontal temperature advection to extreme SAT anomaly development over land and its role is generally stronger in the winter hemisphere.
- For both seasons, over regions with steep topographic slopes such as the Tibetan Plateau, western North America, Greenland, and the Andes, the primary contributor to SAT anomaly growth is adiabatic warming (light green in Figs. 7,c). This process also dominates the JJA anomaly growth in the Russian Far East and Alaska (Fig. 7a), and the DJF anomaly decay over various mountainous regions (Fig. 7d).
- Longwave radiation (orange) generally opposes SAT anomaly growth, most notably over the oceans, and therefore, this term is the strongest damping mechanism over the oceans except for the central and eastern tropical Pacific for both seasons (Figs. 7b,d). Longwave radiation, however, accounts for the warming of summertime arid regions such as the western United States and the Sahel during JJA (Fig. 7a), Australia and southern Africa during DJF (Fig. 7c), and the central and eastern tropical Pacific during both seasons. In contrast, vertical mixing (red) is the largest contributor to extreme SAT anomaly growth over much of the tropical oceans during both seasons, and over the eastern North Atlantic and northern Eurasia during DJF (Figs. 7a,c) and this term dominates the SAT anomaly decay over the central and eastern tropical Pacific, most tropical land areas, and much of North America and northern Eurasia (Figs. 7b,d) for both JJA and DJF. Although not illustrated in Fig. 7, the combination of strong longwave cooling over the oceans and warming due to vertical mixing over land creates the distinctive land–sea contrast pattern of the total diabatic heating.

Our findings underscore the important role that horizontal temperature advection plays in generating anomalously strong SAT anomalies during extreme warming events, which is consistent with earlier studies (Garfinkel and Harnik 2017; Loikith and Neelin 2019; Tamarin-Brodsky et al. 2019, 2020; Linz et al. 2020; Zhang et al. 2022). Especially, our results show that the advection of the climatological temperature by the anomalous wind still warms the SAT even during the decay period, implying that this term is a key process determining the persistence of the extreme SAT anomalies. In addition, we also found that the adiabatic warming over mountain regions and diabatic heating are also important for generating strong SAT anomalies, which agrees with the findings from Röthlisberger and Papritz (2023).

While it is beyond the scope of this study to identify the cause of diabatic heating processes, our results offer some insights. Although the direct effect of shortwave radiative heating on the air temperature is negligible (Figs. 1m and 4m), it can still indirectly influence the SAT anomaly by increasing the skin temperature (Figs. 2c and 5c) and thereby allowing more turbulent vertical mixing to occur within the boundary layer. Such an indirect role of shortwave radiation is expected to be stronger during summer, while during winter, the role of heating due to vertical mixing can be more tied to the vertical relocation of temperature anomalies associated with stronger winter circulation (Clark and Feldstein 2022). The surface heating caused by shortwave radiation can also help explain the longwave radiative warming over summertime dry regions such as central Asia and western North America (Fig. 1n), and southern Africa and Australia (Fig. 4n). Less atmospheric longwave emission is expected with dry atmosphere (Clark and Feldstein 2020b), but because large positive skin temperature anomalies (Figs. 2a and 5a) associated with shortwave flux (Figs. 2c and 5c) would cause an anomalous upward flux of longwave radiation into the atmosphere, longwave flux convergence and SAT warming is expected. Further systematic studies testing such a hypothesis on the root cause of the diabatic heating is necessary. More importantly, our results also imply that future projections of surface heat waves by climate models can be significantly influenced by the parameterization schemes of these diabatic heating processes.

It is our hope that the mechanisms that drive typical extreme warming events, as we documented here, will serve as a benchmark for future studies that seek to determine the processes behind specific extreme events. For example, prior studies have shown that adiabatic warming is an important contributor to summer heat waves over Europe, the Russian Far East, and western North America (Wulff et al. 2017; Zschenderlein et al. 2019; Kim and Lee 2022; Bartusek et al. 2022). In this study, we found that the adiabatic warming typically plays a major role over those regions. Therefore, although the amplitude of the SAT anomalies of those extreme events may have been exceptional, they were likely driven by the same benchmark processes documented here rather than by unusual mechanisms. In addition, our findings that during DJF the SAT anomalies are generally aided by horizontal temperature advection and that they decay through longwave cooling over the ocean and vertical mixing over the land are also consistent with the earlier findings for the NAO and the PNA (Clark and Feldstein 2020a, 2022). In a future study, it would be worthwhile to investigate if and how these benchmark processes can drive SAT extremes of unprecedented magnitudes.

Acknowledgments. We thank Mingyu Park, Changhyun Yoo, Cory Baggett, Michael Goss, Allen Mewhinney, and Pin-Chun Huang for their discussion on this research. The initial version of this manuscript was submitted to Pennsylvania State University as a partial fulfillment of Dong Wan Kim's Ph.D. dissertation. This research was funded by National Science Foundation Grant AGS-1948667.

Data availability statement. The ERA5 data can be downloaded from the ECMWF's webpage: https://confluence.ecmwf.int/display/CKB/How%2Bto%2Bdownload%2BERA5.

REFERENCES

Bartusek, S., K. Kornhuber, and M. Ting, 2022: 2021 North American heatwave amplified by climate change-driven nonlinear interactions. *Nat. Climate Change*, **12**, 1143–1150, https://doi.org/10.1038/s41558-022-01520-4.

Berrisford, P., D. Dee, K. Fielding, M. Fuentes, P. Kållberg, S. Kobayashi, and S. Uppala, 2009: The ERA Interim archive: Version 1.0. ECMWF ERA Rep. Series 1, 20 pp., https://www.ecmwf.int/sites/default/files/elibrary/2009/8173-era-interim-archive.pdf.

Bieli, M., S. Pfahl, and H. Wernli, 2015: A Lagrangian investigation of hot and cold temperature extremes in Europe. *Quart. J. Roy. Meteor. Soc.*, **141**, 98–108, https://doi.org/10.1002/qj.2339.

Clark, J. P., and S. B. Feldstein, 2020a: What drives the North Atlantic Oscillation's temperature anomaly pattern? Part I: The growth and decay of the surface air temperature anomalies. *J. Atmos. Sci.*, **77**, 185–198, https://doi.org/10.1175/JAS-D-19-0027.1.

——, and ——, 2020b: What drives the North Atlantic Oscillation's temperature anomaly pattern? Part II: A decomposition of the surface downward longwave radiation anomalies. *J. Atmos. Sci.*, **77**, 199–216, https://doi.org/10.1175/JAS-D-19-0028.1.

——, and ——, 2022: The temperature anomaly pattern of the Pacific–North American teleconnection: Growth and decay. *J. Atmos. Sci.*, **79**, 1237–1252, https://doi.org/10.1175/JAS-D-21-0030.1.

——, V. Shenoy, S. B. Feldstein, S. Lee, and M. Goss, 2021: The role of horizontal temperature advection in Arctic amplification. *J. Climate*, **34**, 2957–2976, https://doi.org/10.1175/JCLI-D-19-0937.1.

Forget, G., and D. Ferreira, 2019: Global ocean heat transport dominated by heat export from the tropical Pacific. *Nat. Geosci.*, **12**, 351–354, https://doi.org/10.1038/s41561-019-0333-7.

Garfinkel, C. I., and N. Harnik, 2017: The non-Gaussianity and spatial asymmetry of temperature extremes relative to the storm track: The role of horizontal advection. *J. Climate*, **30**, 445–464, https://doi.org/10.1175/JCLI-D-15-0806.1.

Gong, T., S. Feldstein, and S. Lee, 2017: The role of downward infrared radiation in the recent Arctic winter warming trend.

J. Climate, **30**, 4937–4949, https://doi.org/10.1175/JCLI-D-16-0180.1.

Hersbach, H., and Coauthors, 2020: The ERA5 global reanalysis. *Quart. J. Roy. Meteor. Soc.*, **146**, 1999–2049, https://doi.org/10.1002/qj.3803.

Kim, D. W., and S. Lee, 2022: Dynamical mechanism of the summer circulation trend pattern and surface high temperature anomalies over the Russian Far East. *J. Climate*, **35**, 6381–6393, https://doi.org/10.1175/JCLI-D-22-0244.1.

Lau, W. K. M., and K.-M. Kim, 2012: The 2010 Pakistan flood and Russian heat wave: Teleconnection of hydrometeorological extremes. *J. Hydrometeor.*, **13**, 392–403, https://doi.org/10.1175/JHM-D-11-016.1.

Lee, S., T. Gong, S. B. Feldstein, J. A. Screen, and I. Simmonds, 2017: Revisiting the cause of the 1989–2009 Arctic surface warming using the surface energy budget: Downward infrared radiation dominates the surface fluxes. *Geophys. Res. Lett.*, **44**, 10 654–10 661, https://doi.org/10.1002/2017GL075375.

Lesins, G., T. J. Duck, and J. R. Drummond, 2012: Surface energy balance framework for Arctic amplification of climate change. *J. Climate*, **25**, 8277–8288, https://doi.org/10.1175/JCLI-D-11-00711.1.

Li, Q., and S. Lee, 2017: A mechanism of mixed layer formation in the Indo–western Pacific Southern Ocean: Preconditioning by an eddy-driven jet-scale overturning circulation. *J. Phys. Oceanogr.*, **47**, 2755–2772, https://doi.org/10.1175/JPO-D-17-0006.1.

——, ——, and M. Mazloff, 2018: Evidence of jet-scale overturning ocean circulations in Argo float trajectories. *Geophys. Res. Lett.*, **45**, 11 866–11 874, https://doi.org/10.1029/2018GL078950.

Linz, M., G. Chen, B. Zhang, and P. Zhang, 2020: A framework for understanding how dynamics shape temperature distributions. *Geophys. Res. Lett.*, **47**, e2019GL085684, https://doi.org/10.1029/2019GL085684.

Loikith, P. C., and J. D. Neelin, 2019: Non-Gaussian cold-side temperature distribution tails and associated synoptic meteorology. *J. Climate*, **32**, 8399–8414, https://doi.org/10.1175/JCLI-D-19-0344.1.

Röthlisberger, M., and L. Papritz, 2023: Quantifying the physical processes leading to atmospheric hot extremes at a global scale. *Nat. Geosci.*, **16**, 210–216, https://doi.org/10.1038/s41561-023-01126-1.

Seneviratne, S. I., D. Lüthi, M. Litschi, and C. Schär, 2006: Land–atmosphere coupling and climate change in Europe. *Nature*, **443**, 205–209, https://doi.org/10.1038/nature05095.

Setchell, H., 2020: L137 model level definitions. ECMWF, accessed 26 April 2023, https://confluence.ecmwf.int/display/UDOC/L137+model+level+definitions.

Tamarin-Brodsky, T., K. Hodges, B. J. Hoskins, and T. G. Shepherd, 2019: A dynamical perspective on atmospheric temperature variability and its response to climate change. *J. Climate*, **32**, 1707–1724, https://doi.org/10.1175/JCLI-D-18-0462.1.

——, ——, ——, and ——, 2020: Changes in Northern Hemisphere temperature variability shaped by regional warming patterns. *Nat. Geosci.*, **13**, 414–421, https://doi.org/10.1038/s41561-020-0576-3.

Wulff, C. O., R. J. Greatbatch, D. I. V. Domeisen, G. Gollan, and F. Hansen, 2017: Tropical forcing of the summer East Atlantic pattern. *Geophys. Res. Lett.*, **44**, 11 166–11 173, https://doi.org/10.1002/2017GL075493.

Yeo, S.-R., S.-W. Yeh, and W.-S. Lee, 2019: Two types of heat wave in Korea associated with atmospheric circulation pattern. *J. Geophys. Res. Atmos.*, **124**, 7498–7511, https://doi.org/10.1029/2018JD030170.

Zhang, B., M. Linz, and G. Chen, 2022: Interpreting observed temperature probability distributions using a relationship between temperature and temperature advection. *J. Climate*, **35**, 705–724, https://doi.org/10.1175/JCLI-D-20-0920.1.

Zschenderlein, P., A. H. Fink, S. Pfahl, and H. Wernli, 2019: Processes determining heat waves across different European climates. *Quart. J. Roy. Meteor. Soc.*, **145**, 2973–2989, https://doi.org/10.1002/qj.3599.